Japanese Journal of Applied Physics 51 (2012) 054102 **REGULAR PAPER**
DOI: 10.1143/JJAP.51.054102

Buffer-Related Degradation Aspects of Single and Double-Heterostructure Quantum Well InAlN/GaN High-Electron-Mobility Transistors

Jan Kuzmik[1,2]*, Stanislav Vitanov[2], Christian Dua[3], Jean-Francois Carlin[4], Clemens Ostermaier[5], Alexander Alexewicz[5], Gottfried Strasser[5], Dionyz Pogany[5], Erich Gornik[5], Nicolas Grandjean[4], Sylvain Delage[3], and Vassil Palankovski[2]

[1] *Institute of Electrical Engineering, Slovak Academy of Sciences, Dubravska Cesta 9, 84104 Bratislava, Slovakia*
[2] *Advanced Materials and Device Analysis Group, Institute for Microelectronics, Vienna University of Technology, Gusshausstr. 27-29, 1040 Vienna, Austria*
[3] *Alcatel-Thales III–V Lab, Route de Nozay, 91460 Marcoussis, France*
[4] *Institute of Condensed Matter Physics, Ecole Polytechnique Federale de Lausanne, 1015 Lausanne, Switzerland*
[5] *Institute of Solid State Electronics, Vienna University of Technology, Floragasse 7, 1040 Vienna, Austria*

Received November 11, 2011; accepted March 2, 2012; published online May 1, 2012

We experimentally prove the viability of the concept of the double-heterostructure quantum well InAlN/GaN high-electron-mobility transistor (HEMT) for the device higher robustness and reliability. In the single quantum well InAlN/GaN HEMTs, the intrinsic channel resistance increases by 300% after 1 h off-state stress; much less degradation is observed in the double-heterostructure device with an AlGaN back barrier. Physics-based device simulation proves that the back barrier blocks the rate of carrier injection into the device buffer. However, whatever the quantum well design is, the energy of the injected electrons in the buffer of InAlN/GaN-based HEMTs is higher than that in the buffer of AlGaN/GaN HEMTs. This energy may be sufficient for releasing hydrogen from GaN point defects. © 2012 The Japan Society of Applied Physics

1. Introduction

InAlN/GaN high-electron-mobility transistors (HEMTs) were shown to be an excellent alternative to AlGaN/GaN HEMTs for ultrahigh-frequency[1,2] and power[3] applications. It was emphasized that the channel electron velocity in the InAlN/GaN system is substantially higher as it is observed in AlGaN/GaN HEMTs.[2] Simultaneously, it was shown that InAlN/GaN HEMTs can operate at 1000 °C without permanent damage.[4] The excellent device performance and stability may stem from the lattice matching of the InAlN barrier to GaN.[5] Elsewhere, it was shown that an electric-field-driven relaxation of the material lattice observed in AlGaN/GaN (so-called inverse piezo-electric effect)[6] is mitigated in lattice-matched InAlN/GaN HEMTs.[7] On the other hand, from the point of view of gate leakage, InAlN/GaN HEMTs seem to be less matured when compared with their AlGaN/GaN counterparts because of the high tunneling current component.[8] Gate insulation may be a solution for this particular problem.[9] In this paper, we address reliability aspects of InAlN/GaN HEMTs in relation to the possible hot electron-related degradation of the buffer layer. The degradation of the buffer layer has recently been indicated as one of the most critical aspects of the InAlN/GaN HEMT performance.[7]

For AlGaN/GaN HEMTs, it has been shown that the electrical stress at the drain voltage $V_{DS} = 20$ V and gate voltage V_{GS} close to the pinch-off can reduce the device transconductance and degrades the GaN buffer.[10,11] The effect could be explained by the high electric field under the drain side of the gate giving a sufficient energy to electrons to dehydrogenate point defects in the buffer.[10,11] Hydrogen is naturally present during the III-N epitaxial growth and can be attached or subsequently released from Ga vacancies.[10–12] The release of one or more hydrogen atoms by energetic electrons gives rise to (more) negatively charged complexes with an acceptor-like nature.[10,11] Those changes are not spontaneously reversible and, consequently, the HEMT threshold voltage V_T can be permanently shifted and, more importantly, the channel mobility can be degraded owing to an enhanced Coulomb scattering.[10,11] It was shown that the hydrogen removal energy from the single hydrogenated Ga vacancy ranges from 0.72 to 3.55 eV depending on the position of the Fermi level E_F in the buffer.[12] A better confinement of electrons in the AlGaN/GaN HEMT channel and a reduced rate of carrier injection in the GaN buffer were observed for the double-heterostructure quantum well (DHQW) system by applying the AlGaN back barrier.[13,14] Consequently, a lower subthreshold drain leakage[13,14] and a reduced trapping in the buffer[14] could be obtained. The AlGaN back barrier has also been tested in InAlN/GaN HEMTs, resulting in an improved device *RF* performance and reduced short-channel effects.[15] In this study, we evaluated hot-electron injection effects in the buffer of InAlN/GaN HEMTs by two-dimensional hydrodynamic transport simulation and experiment. In particular, we analyzed why InAlN/GaN HEMTs seem to be more vulnerable to the off-state stress than their AlGaN/GaN-based counterparts.[7] The approach of InAlN/(AlN)/GaN/AlGaN DHQW HEMTs is tested for a higher device robustness and less degradation in the system.

2. Model and Experimental Methods

We performed hydrodynamic simulations with our two-dimensional (2D) device simulator Minimos-NT, which already has been successfully employed for the analysis of GaN-based HEMTs.[16,17] The hydrodynamic transport model is derived from the Boltzmann equation by taking into account the first four moments of the distribution function. A system of partial differential equations, namely, Poisson, current continuity, and energy balance equations for electrons, is solved self-consistently. Holes are neglected in the model.

$In_{0.17}Al_{0.83}N$ (13 nm)/AlN (1 nm)/GaN (1.2 μm) single quantum well (SQW) HEMT structures were grown by MOCVD on sapphire substrates. InAlN of 17% In content was chosen to induce lattice matching to GaN.[5] A thin AlN interlayer is used to improve the carrier mobility in the channel.[18] The sum of polarization charges at AlN interfaces equals the polarization charge at the InAlN/GaN

*E-mail address: Jan.Kuzmik@savba.sk

 © 2012 The Japan Society of Applied Physics

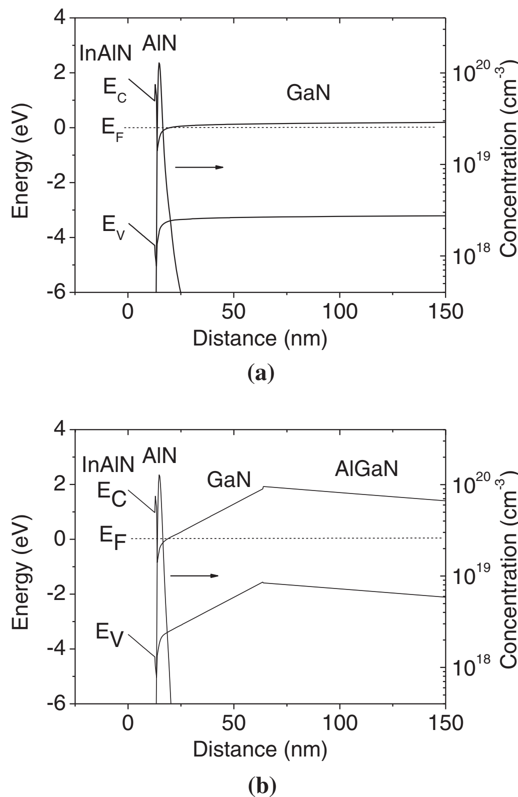

Fig. 1. Calculated band diagrams of (a) SQW and (b) DHQW $In_{0.17}Al_{0.83}N/GaN$ HEMTs in equilibrium. The Al molar fraction in the AlGaN back barrier of the DHQW is 4%. For clarity, only top 150 nm is shown.

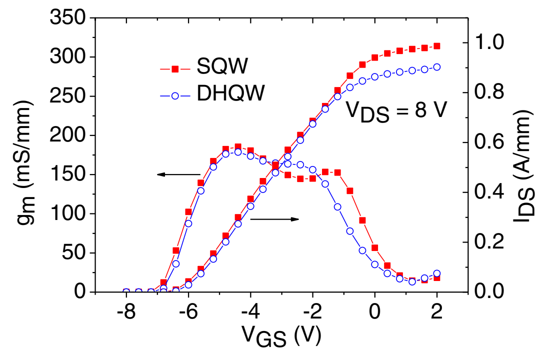

Fig. 2. (Color online) Transfer and transconductance characteristics of InAlN/GaN SQW and DHQW HEMTs at $V_{DS} = 8$ V.

interface;[19] thus, in simulations, we consider 14 nm InAlN without the interlayer. In the alternative DHQW structures, a 50-nm-thick GaN layer and a 310 nm $Al_{0.04}Ga_{0.96}N$ back barrier were inserted between the GaN buffer and the AlN spacer. To eliminate a possible detrimental effect of the low thermal conductivity of AlGaN, the thickness of AlGaN was only 310 nm. As expected, the calculated SQW and DHQW band diagrams shown in Figs. 1(a) and 1(b) indicate that electrons in the DHQW are better confined owing to a raised conduction band E_C in the GaN channel, which is due to an additional negative polarization charge at a GaN/AlGaN junction of the DHQW structure shown in Fig. 1(b). The Hall experiment showed identical data for both structures with an electron mobility $\mu \sim 560\,\mathrm{cm^2\,V^{-1}\,s^{-1}}$ and a sheet carrier concentration $n_s \sim 2.2 \times 10^{13}\,\mathrm{cm^{-2}}$. It was shown elsewhere that the experimental n_s depends on the condition of the InAlN surface[20] and/or on conditions during the epi-structure growth.[21] To obtain the best agreement of the model with the experimental n_s, we used an E_C surface potential of 1.8 eV. In this case, by integrating the calculated volumetric carrier concentration profiles, we obtained $n_s = 2.4 \times 10^{13}\,\mathrm{cm^{-2}}$ for the SQW and about 8% less sheet concentration $n_s = 2.2 \times 10^{13}\,\mathrm{cm^{-2}}$ for the DHQW HEMT. The invariant experimental n_s can be explained by the inaccuracy of the Hall experiment and/or of the InAlN barrier thicknesses. Still, as shown in Fig. 1(b), even the relatively low Al mole fraction in the back barrier is sufficient for creating a clear back barrier potential reaching almost 2 eV at the GaN/AlGaN junction. Device processing included mesa etching using Ar-based RIE (~250 nm deep) and Ti/Al/Ni/Au ohmic and Ni/Au Schottky barrier contacts defined by e-beam lithography. The gate length is 0.25 µm, and the gate-to-drain distance is ~1.5 µm. All devices were unpassivated.

InAlN/GaN-based (both SQW and DHQW) HEMTs were degraded by applying a 1 h off-state stress with $V_{GS} = -8$ V and $V_{DS} = 20$ V. The output characteristics were measured before and after the stress. For the extraction of the source (R_S), drain (R_D) as well as intrinsic open channel (R_{CHIO}) resistances, we modified a method that was formerly developed for GaAs metal–semiconductor field-effect transistors (MESFETs).[22] In the former method, the total source-to-drain resistance $R_T = R_S + R_D + R_{CHI}$ is measured as a function of

$$V_x = \left[1 - \left(\frac{V_{bi} - V_{GS}}{V_{bi} - V_T}\right)^{1/2}\right]^{-1}, \quad (1)$$

where R_{CHI} is the channel resistance, V_{bi} is the Schottky contact barrier height, and V_x quantifies the modulation of R_{CHI} by V_{GS}, i.e., $V_x = R_{CHI}/R_{CHIO}$. In an acquired linear dependence, a graph extrapolation to $V_x = 0$ gives $R_S + R_D$, and the slope of the line provides R_{CHIO}.[22] However, in GaN HEMTs, a two-dimensional electron gas density depends linearly on V_{GS}.[5] Consequently, for the HEMT analysis, we obtain R_{CHI}, which varies proportionally to

$$V_x = \left(1 - \frac{V_{bi} - V_{GS}}{V_{bi} - V_T}\right)^{-1}. \quad (2)$$

3. Results and Discussion

Figure 2 shows source–drain current I_{DS} transfer and transconductance g_m characteristics of both InAlN/GaN-based HEMTs investigated. Slightly lower I_{DS} and g_m values on DHQW HEMTs were obtained owing to an ohmic contact resistance $R_C \sim 0.5\,\Omega\,\mathrm{mm}$, which is higher than $R_C \sim 0.3\,\Omega\,\mathrm{mm}$ for SQW HEMTs. On the other hand, almost the same threshold voltage $V_T \sim -6.3$ V could be extracted for both devices. The nonintentionally thicker InAlN barrier (by about 5%) of the DHQW system is a possible explanation for the almost identical V_T. The AlGaN back barrier reduces the rate of carrier injection into the buffer, which is reflected in the subthreshold output characteristics of the DHQW HEMT shown in Fig. 3. For $V_{GS} = -8$ V, Fig. 3 shows almost three orders of magnitude reductions in the gate I_G and drain I_D off-state leakage

© 2012 The Japan Society of Applied Physics

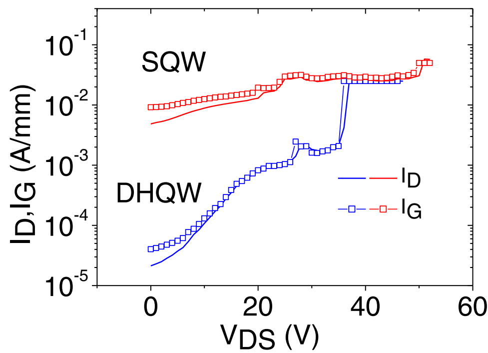

Fig. 3. (Color online) Subthreshold output and breakdown characteristics of InAlN/GaN SQW and DHQW HEMTs at $V_{GS} = -8$ V.

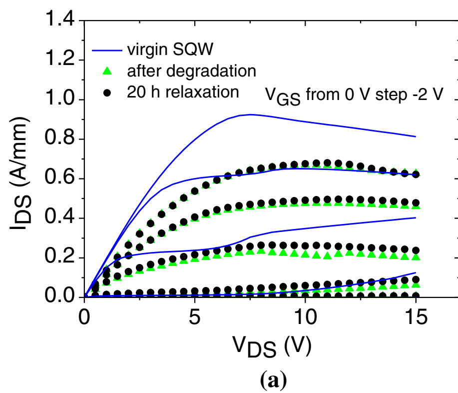

(a)

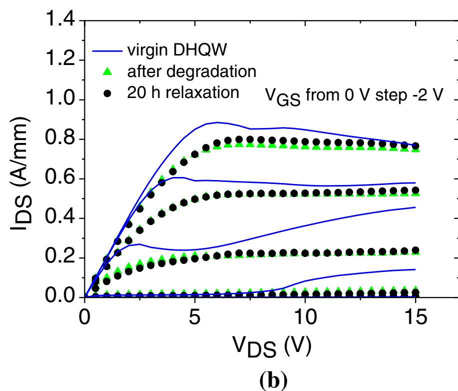

(b)

Fig. 4. (Color online) Output characteristics of InAlN/GaN (a) SQW and (b) DHQW HEMTs in the virgin stage, immediately after the off-state degradation and after the consecutive 20 h relaxation.

currents when compared with those of the SQW HEMT. However, owing to electron tunneling through the InAlN barrier,[8] the leakage currents were dominated by I_G and, consequently, the off-state breakdown appeared at a relatively low $V_{DS} \sim 35$ V. A rather high gate leakage (>1 mA/mm) in InAlN/GaN HEMTs was reported also elsewhere;[1] better Schottky contacts can be expected after using an oxygen plasma treatment[1] or by reducing the threading dislocation density in InAlN.[23]

Figure 4 shows the evolution of the output characteristics of InAlN/GaN (a) SQW and (b) DHQW HEMTs before and after the degradation stress and after a 20 h relaxation (at no bias) following the stress. A strong reduction in I_{DS} (by ~30% at $V_{GS} = 0$ V) was observed after the stress for

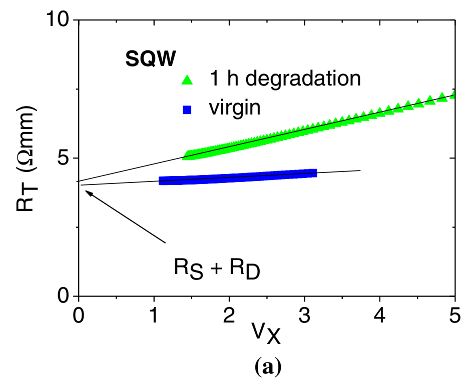

(a)

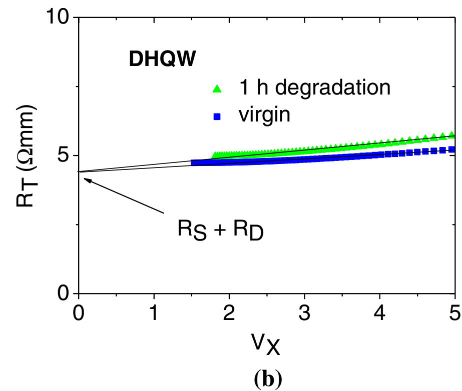

(b)

Fig. 5. (Color online) Extraction of the parasitic resistances and intrinsic channel resistance (slope of the line) of InAlN/GaN (a) SQW and (b) DHQW HEMTs. Measured points represent HEMT output resistances at $V_{DS} = 0.5$ V, $V_x = \{1 - [(V_{bi} - V_{GS})/(V_{bi} - V_T)]\}^{-1}$.

the SQW HEMT. In contrast, for the DHQW HEMT, I_{DS} decreased by ~10% only [see Fig. 4(b)]. Changes were found irreversible after 20 h [see Figs. 4(a) and 4(b)] and also after several weeks (not shown). Further analysis of the R_S, R_D, and R_{CHIO} of the virgin and degraded SQW HEMTs indicated that while R_{CHIO} increased by about 300%, access resistances remained practically intact after the stress [see Fig. 5(a)]. Simultaneously, we observed only a low positive shift ~0.15 V in V_T. These findings strongly indicate that the I_{DS} reduction could be explained by the degraded carrier mobility in the intrinsic part of the channel. We may suggest that the enhanced Coulomb scattering on charged defects in the GaN buffer affects the carrier mobility. Similarly, as proposed for AlGaN/GaN HEMTs,[10,11] charging may take place owing to the hot electron injection in the buffer layer and to the release of hydrogen atoms. This mechanism may be diminished by using the back barrier as it was confirmed by analyzing the R_S, R_D, and R_{CHIO} of the DHQW InAlN/GaN HEMT [see Fig. 5(b)]. In this case, $R_S + R_D$ also remains intact; however, R_{CHIO} is increased only by about 60%. The normalized values of R_{CHIO} and I_{DS} at $V_{GS} = 0$ V for both devices before and after the stress are summarized in Table I. We finally note that for both devices, a kink effect was observed in the virgin state particularly at $V_{GS} = -4$ V, which disappeared after the stress (see Fig. 4). A similar effect has been studied earlier and explained by the injection and trapping of electrons in the buffer layer.[24]

In Figs. 6(a)–6(c), we show results of the 2D physics-based device simulation for a hypothetical $Al_{0.22}Ga_{0.78}N$/GaN HEMT in comparison with experimental SQW and

 © 2012 The Japan Society of Applied Physics

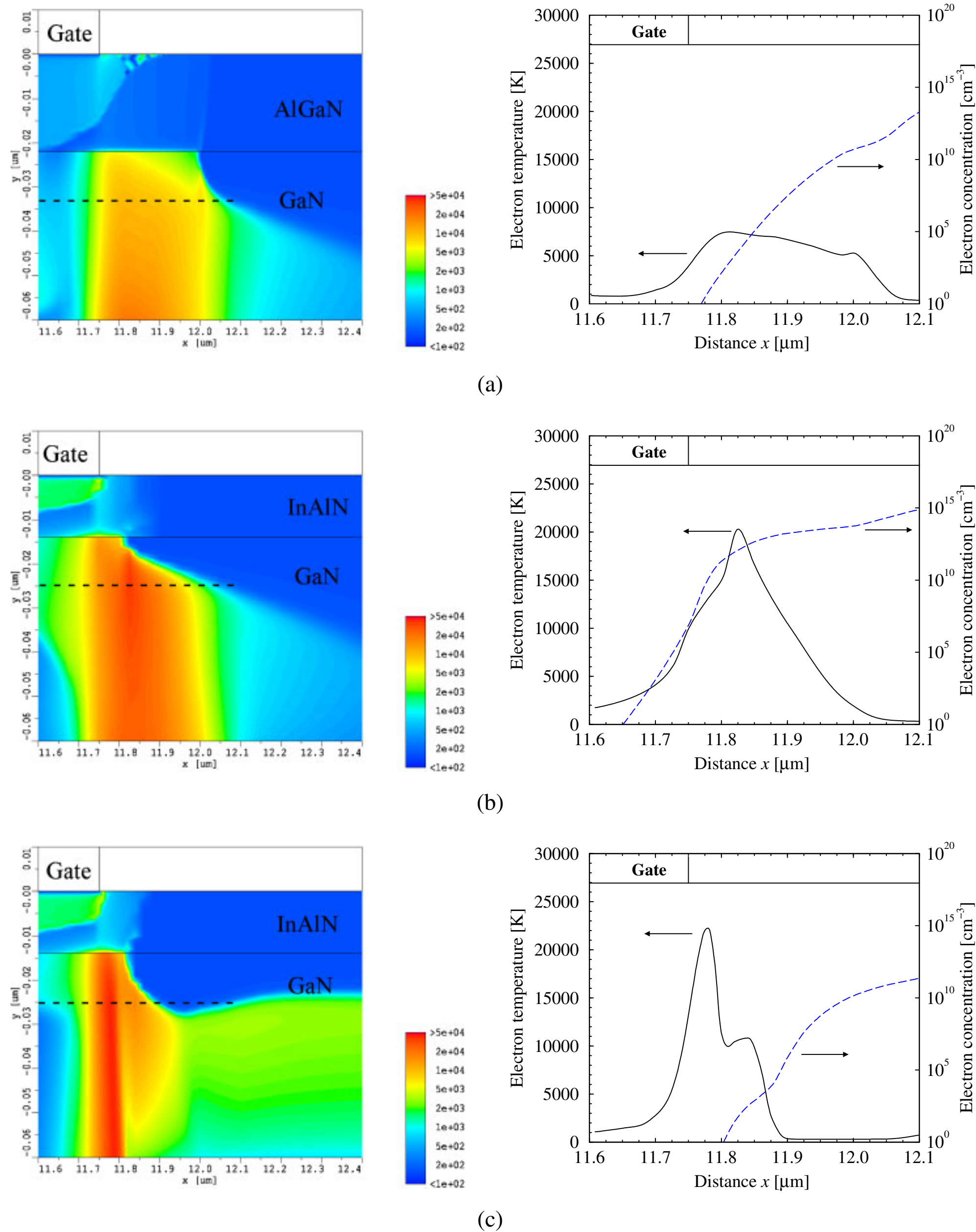

Fig. 6. (Color online) Calculated 2D electron temperature maps at the drain side of the gate (left panel) and cross sections of the electron concentration and temperature in the buffer (right panel) of (a) $Al_{0.22}Ga_{0.78}N$ (22 nm)/GaN SQW, (b) $In_{0.17}Al_{0.83}N$ (14 nm)/GaN SQW, and (c) $In_{0.17}Al_{0.83}N$ (14 nm)/GaN/$Al_{0.04}Ga_{0.96}N$ DHQW HEMTs at $V_{GS} = -8$ and $V_{DS} = 20$ V. Dashed lines in the maps indicate the positions of the cross sections along the GaN channel at a distance of 11 nm from the QW. The color electron temperature scale is shown in Kelvins. All devices have gate lengths of 0.25 µm, and source-to-gate and gate-to-drain distances are 1.5 µm.

Table I. Normalized I_{DS} at $V_{GS} = 0$ V and R_{CHIO} of InAlN/GaN SQW and DHQW HEMTs before and after the degradation stress.

	SQW		DHQW	
	I_{DS}	R_{CHIO}	I_{DS}	R_{CHIO}
Virgin	1	1	1	1
Degraded	0.7	4	0.9	1.6

DHQW $In_{0.17}Al_{0.83}N$/GaN HEMTs. First, we compared a hypothetical AlGaN/GaN SQW HEMT [see Fig. 6(a)] with the experimental InAlN/GaN SQW HEMT, as shown in Fig. 6(b). For the AlGaN/GaN HEMT, we assumed a geometry similar to that of the InAlN/GaN device. To obtain the same V_T in the $Al_{0.22}Ga_{0.78}N$/GaN HEMT as that in $In_{0.17}Al_{0.83}N$/GaN we chose the thickness of the AlGaN layer to be 22 nm. Detailed images for $V_{DS} = 20$ and $V_{GS} = -8$ V indicate that a much higher energy of injected electrons could be expected in the buffer layer of the InAlN/GaN HEMT, as observed in its AlGaN/GaN counterpart. In particular, the "hot spot" in the buffer of the AlGaN/GaN HEMT shows an T_e of only about 7000 K (corresponding to $\sim$0.95 eV energy) in comparison with $T_e \sim 20000$ K for the InAlN/GaN HEMT. The indicated T_e in AlGaN/GaN corresponds only to the onset of the possible dehydrogenation of defects in the GaN buffer, which has a minimum required energy of $\sim$0.72 eV.[12] On the other hand, hot electrons in the InAlN/GaN HEMT buffer seem to have a sufficient energy for releasing hydrogen atoms. The higher T_e in the InAlN/

 © 2012 The Japan Society of Applied Physics

GaN HEMT is due to the higher polarization fields in InAlN/GaN HEMTs than in AlGaN/GaN HEMTs.[25] The polarization in the GaN-based QW is related to n_s, and the depletion of the channel requires the proportional application of a sufficient gate bias to the polarization field.[25] The resulting vertical electric field in InAlN/GaN HEMTs under the off-state condition deflects the channel electrons with higher energies in the buffer. Consequently, the buffer layer in InAlN/GaN HEMTs may be more vulnerable to degradation than that in AlGaN/GaN HEMTs.

Furthermore, we compared SQW and DHQW InAlN/GaN HEMTs to study the effect of the AlGaN back barrier [see Figs. 6(b) and 6(c)]. The maximal T_e seems to be not significantly affected by the presence of the back barrier; however, as indicated by lateral cross sections (right panel of Fig. 6), there is a much lower concentration of injected electrons in the DHQW HEMT than in the SQW HEMT. This may explain the higher stability of DHQW InAlN/GaN HEMTs. Moreover, besides the blocking effect of the back barrier on the injection of hot electrons, the increased $E_C - E_F$ in the buffer layer of the DHQW HEMT increases the electron energy required for the dehydrogenation of point defects.[12]

We note that to explain the observed changes in the studied HEMTs, alternative mechanisms related to the charging of pre-existing traps in the buffer[14,26] or at the surface of the barrier layer[27] may be considered. However, in our case, at least in a time scale of weeks, we observe irreversible effects, which is in contrast to the transient effects expected for a sole electron trapping.[26,27] Also, in our experiment, the deduced changes in R_{CHIO} are related to the intrinsic part of the transistor, which would exclude effects in the surface access regions. Finally, while there is a minimum energy required to release hydrogen from Ga vacancies,[12] for the electron trapping, the dependence of the device performance on the density of injected electrons seems to be more crucial.[26] Therefore, we assume a dominant role of the hot-electron dehydrogenation of defects in the buffer and only a minor role of pre-existing traps in the observed permanent degradations. This study was performed on unpassivated devices. Investigations of degradation mechanisms in DHQW InAlN/GaN HEMTs with passivated surface and/or insulated gates are ongoing.

4. Conclusions

We studied the electrical performance and degradation mechanisms in InAlN/GaN HEMTs with and without an AlGaN back barrier. We showed the viability of the DHQW concept with improvements in the HEMT off-state characteristics and in the device stability when compared with the SQW InAlN/GaN HEMT. The 2D physics-based model confirmed the better confinement of carriers in the proposed DHQW structure than in SQW HEMTs with a lower rate of carrier injection in the buffer layer. The model also indicated that the buffer layer in InAlN/GaN-based HEMTs may be more vulnerable to hot-electron degradation as in AlGaN/GaN HEMTs and consequently may require a more careful design.

Acknowledgments

The support of the European Commission through the MORGAN project, contract FP7 NMP IP 214610, the Austrian Science Funds (FWF), Project START Y247-N13, and the Slovak Research and Development Agency under the contract No. APVV-0104010 is acknowledged.

1) D. S. Lee, J. W. Chung, H. Wang, X. Gao, S. Guo, P. Fay, and T. Palacios: IEEE Electron Device Lett. **32** (2011) 755.
2) H. Sun, A. R. Alt, H. Benedickter, E. Feltin, J.-F. Carlin, M. Gonschorek, N. R. Grandjean, and C. R. Bolognesi: IEEE Electron Device Lett. **31** (2010) 957.
3) N. Sarazin, E. Morvan, M. A. di Forte Poisson, M. Oualli, C. Gaquière, O. Jardel, O. Drisse, M. Tordjman, M. Magis, and S. L. Delage: IEEE Electron Device Lett. **31** (2010) 11.
4) F. Medjdoub, J.-F. Carlin, M. Gonschorek, E. Feltin, M. A. Py, D. Ducatteau, C. Gaquière, N. Grandjean, and E. Kohn: IEDM Tech. Dig., 2006, p. 927.
5) J. Kuzmík: Semicond. Sci. Technol. **17** (2002) 540.
6) J. Joh and J. A. del Alamo: IEEE Electron Device Lett. **29** (2008) 287.
7) J. Kuzmik, G. Pozzovivo, C. Ostermaier, G. Strasser, D. Pogany, E. Gornik, J.-F. Carlin, M. Gonschorek, E. Feltin, and N. Grandjean: J. Appl. Phys. **106** (2009) 124503.
8) D. Donoval, A. Chvála, R. Šramatý, J. Kováč, J.-F. Carlin, N. Grandjean, G. Pozzovivo, J. Kuzmík, D. Pogany, G. Strasser, and P. Kordoš: Appl. Phys. Lett. **96** (2010) 223501.
9) J. Kuzmik, G. Pozzovivo, S. Abermann, J.-F. Carlin, M. Gonschorek, E. Feltin, N. Grandjean, E. Bertagnolli, G. Strasser, and D. Pogany: IEEE Trans. Electron Devices **55** (2008) 937.
10) T. Roy, Y. S. Puzyrev, B. R. Tuttle, D. M. Fleetwood, R. D. Schrimpf, D. F. Brown, U. K. Mishra, and S. T. Pantelides: Appl. Phys. Lett. **96** (2010) 133503.
11) Y. S. Puzyrev, T. Roy, M. Beck, B. R. Tuttle, R. D. Schrimpf, D. M. Fleetwood, and S. T. Pantelides: J. Appl. Phys. **109** (2011) 034501.
12) A. F. Wright: J. Appl. Phys. **90** (2001) 1164.
13) E. Bahat-Treidel, O. Hilt, F. Brunner, J. Würfl, and G. Tränkle: IEEE Trans. Electron Devices **55** (2008) 3354.
14) A. Vescan, H. Hardtdegen, N. Ketteniß, M. Eickelkamp, A. Noculak, J. Goliasch, M. v. d. Ahe, H. L. Bay, T. Schäpers, H. Kalisch, D. Grützmacher, and R. H. Jansen: Phys. Status Solidi C **6** (2009) S1003.
15) D. S. Lee, X. Gao, S. Guo, and T. Palacios: IEEE Electron Device Lett. **32** (2011) 617.
16) S. Vitanov, V. Palankovski, S. Maroldt, and R. Quay: Solid-State Electron. **54** (2010) 1105.
17) S. Vitanov, V. Palankovski, G. Pozzovivo, J. Kuzmik, and R. Quay: Ext. Abstr. European Workshop Heterostructure Technology (HETECH), 2008, p. 159.
18) M. Gonschorek, J.-F. Carlin, E. Feltin, M. A. Py, and N. Grandjean: Appl. Phys. Lett. **89** (2006) 062106.
19) M. Gonschorek, J.-F. Carlin, E. Feltin, M. A. Py, N. Grandjean, V. Darakchieva, B. Monemar, M. Lorenz, and G. Ramm: J. Appl. Phys. **103** (2008) 093714.
20) Md. T. Hasan, H. Tokuda, and M. Kuzuhara: Appl. Phys. Lett. **99** (2011) 132102.
21) J. H. Leach, X. Ni, X. Li, M. Wu, Ü. Özgür, H. Morkoç, L. Zhou, D. A. Cullen, D. J. Smith, H. Cheng, Ç. Kurdak, J. R. Meyer, and I. Vurgaftman: J. Appl. Phys. **107** (2010) 083706.
22) M. Shur: *GaAs Devices and Circuits* (Plenum, New York, 1987) p. 368.
23) J. Song, F. J. Xu, X. D. Yan, F. Lin, C. C. Huang, L. P. You, T. J. Yu, X. Q. Wang, B. Shen, K. Wei, and X. Y. Liu: Appl. Phys. Lett. **97** (2010) 232106.
24) G. Meneghesso, F. Rossi, G. Salvati, M. J. Uren, E. Muñoz, and E. Zanoni: Appl. Phys. Lett. **96** (2010) 263512.
25) J. Kuzmik: IEEE Electron Device Lett. **22** (2001) 510.
26) K. Horio and A. Nakajima: Jpn. J. Appl. Phys. **47** (2008) 3428.
27) J. Kuzmik, J.-F. Carlin, M. Gonschorek, A. Kostopoulos, G. Konstantinidis, G. Pozzovivo, S. Golka, A. Georgakilas, N. Grandjean, G. Strasser, and D. Pogany: Phys. Status Solidi A **204** (2007) 2019.

© 2012 The Japan Society of Applied Physics